Stepwise palaeoclimate change across the Eocene–Oligocene transition recorded in continental NW Europe by mineralogical assemblages and d 15 N org (Rennes Basin, France)

Romain Tramoy, Marie Salpin, Johann Schnyder, Alain Person, Mathieu Sebilo, Johan Yans, Véronique Vaury, Jérôme Fozzani, Hugues Bauer

Stepwise paleoclimate change across the Eocene-Oligocene Transition recorded in continental NW Europe by mineralogical assemblages and $\delta^{15}N_{org}$ (Rennes Basin, France).

Romain Tramoy[1]*, Marie Salpin[1], Johann Schnyder[1], Alain Person[1], Mathieu Sebilo[2], Johan Yans[3], Véronique Vaury[2], Jérôme Fozzani, J.[1], Hugues Bauer[4]

[1]*Sorbonne Universités, UPMC Univ Paris 06, CNRS, Institut des Sciences de la Terre de Paris (iSTeP), 4 place Jussieu 75005 Paris, France.*

[2]*Sorbonne Universités, UPMC Univ Paris 06, CNRS, Institute of Ecology and Environmental Sciences (IEES), 4 place Jussieu 75005 Paris, France.*

[3]*Université de Namur, Department of Geology, NaGRIDD, 61 rue de Bruxelles, 5000 Namur, Belgium.*

[4]*Bureau de Recherches Géologiques et Minières (BRGM), 3 av. Claude Guillemin, 45060 Orléans 5 Cedex2, France*

**Corresponding author: Romain Tramoy. e-mail address: romain.tramoy@upmc.fr (+33 6 76 28 08 38)*

Running Head: Paleoclimate change at the Eocene-Oligocene transition

Abstract

The Eocene-Oligocene Transition (EOT, ~34Ma) is the largest global cooling of the Cenozoic Era and led the Earth climatic system to change from a greenhouse to icehouse mode. Well documented in marine settings, the few studies focusing on continental environments demonstrated regional heterogeneities. The study core CDB1, located in the Rennes Basin (Western France), is a unique terrestrial (lacustrine-palustrine) record made of well-preserved and terrestrial-derived organic-rich sediments encompassing the EOT. Clay minerals and the first organic nitrogen isotopes ($\delta^{15}N_{org}$) record of terrestrial origin for this period are used to reconstruct paleoclimate changes across this key interval. As suggested in

worldwide marine environmental and few continental records, a stepwise transition from warm/humid conditions in the Late Eocene to cooler/drier conditions in the Early Oligocene is confirmed in the area. In addition, an episode of drier conditions in the Late Eocene and humid/dry cycles in the Early Oligocene are suggested.

Keywords

Eocene, Oligocene, Terrestrial Organic Matter (Type III), Paleoclimate, Clay minerals

Introduction

The EOT is marked by a global drastic cooling (4~6 °C) that led the Earth climatic system to evolve from a "greenhouse" to an "icehouse" mode (Kennett and Shackleton, 1976; Zachos, 2001; Lear et al., 2008). This cooling is well documented in marine environments from around the world using elemental and isotopic geochemistry (Zachos, 2001; Katz et al., 2008; Lear et al., 2008; Bohaty et al., 2012; Wade et al., 2012) as well as clay mineralogy (Ehrmann et al., 1992). Many authors have suggested that this global cooling was associated with enhanced seasonality (Ivany et al., 2000; Mosbrugger et al., 2005; Eldrett et al., 2009; Wade et al., 2012; Hren et al., 2013). However, less studies focused on detailed continental records during this major climate change, while they pointed to large heterogeneities in America and Western Europe (Cavagnetto and Anadón, 1996; Mosbrugger et al., 2005; Dupont-Nivet et al., 2007; Sheldon, 2009).

In North-West Europe, previous works have suggested humid/warm tropical conditions from the Ypresian to the Bartonian during which subtropical climate established, whereas the Oligocene was characterized by temperate climate (Ollivier-Pierre et al., 1987, 1993). The CDB1-core drilled in the Rennes Basin (Western France) in 2010, provides the opportunity to

complete and refine the continental record of the area during the EOT. It consists of ~300 m of very well-preserved organic-rich lacustrine sediments, that encompass the Late Eocene to Oligocene series (Bauer et al., 2010, Bauer et al. accepted).

Only few studies have successfully employed bulk organic nitrogen isotopes ($\delta^{15}N_{org}$) in a terrestrial setting as a paleoclimatic proxy in pre-quaternary times (Storme et al., 2012), while clay minerals are commonly used for paleoclimatic reconstructions as they may be associated to inland hydrolysis conditions (Chamley, 1989; Schnyder et al., 2006; Dera et al., 2009). The use of $\delta^{15}N_{org}$ as presented here for pre-quaternary times is relatively new. It is thought that the relative openness of the N-cycle – mostly driven by water availability – at the soil/plant interface controls $\delta^{15}N_{org}$ values: drier conditions lead to higher $\delta^{15}N_{org}$ values (open N-cycle) and conversely (Handley et al., 1999; Swap et al., 2004; Liu and Wang, 2008). In this paper, we applied those concepts to a terrestrial $\delta^{15}N_{org}$ data set, and combined it to the analysis of clay minerals in order to reconstruct paleoclimates.

Geological settings

The NNW-SSE trending graben-type Rennes Basin (10km long; 2km width) is located east of the Armorican Massif along the Pont Péan fault structure (Figure 1; Jaeger, 1967; Ollivier-Pierre et al., 1993). Cenozoic basins of the Armorican Massif are related to the extension phase that affected Western Europe during the Upper Eocene and Oligocene (Esteoule-Choux et al., 1988), leading to the initiation of large rift structures in France and Germany (Bergerat, 1987; Dèzes et al., 2004).

In 2010, the CDB1 core was drilled under the guidance of the French Geological Survey (BRGM). The core was 675 m long including 270 m of Neoproterozic folded sediments as the basement for the overlying 405 m of Cenozoic deposits (Figure 2). The Cenozoic sediments consist of ~300 m of well-preserved organic-rich laminated and massive clays,

suggesting lacustrine to palustrine environments, respectively. The palynological content revealed an organic matter mainly of terrestrial origin, with macrophytes in palustrine environments and extra-palustrine debris from the surrounding vegetation in lacustrine environments (Bauer et al., 2010; Bauer et al. accepted). According to palynomorphs associations, the Eocene-Oligocene boundary was firstly identified around -195 m (Bauer et al., 2010; Bauer et al. accepted), confirmed by magneto- and cyclostratigraphic analyses that positioned the boundary between -205 and -195 m (Boulila et al. in prep.).

Methods

Mineralogy

Bulk mineralogy and clay mineral associations were identified by X-ray diffraction (XRD) using a Bruker D2 phaser X-ray powder diffractometer equipped with a LynxEye detector (CuKα radiation, λ=1.54Å and Ni filter). From -405 m to -66 m, bulk mineralogy was analyzed on 425 samples within Cenozoic deposits (resolution ~0.8 m), whereas clay minerals were analyzed on 244 samples (resolution ~1.30 m). Oriented mounts were prepared for clay minerals analyses and three X-ray diagrams per sample were performed following the analytical procedure described in Moore and Reynolds (1997). Semi-quantitative proportions of the identified minerals were obtained using MacDiff® 4.2.5 software.

Organic geochemistry

Total Organic Carbon (TOC) values, Hydrogen Index (HI) and Oxygen Index (OI) were determined by Rock-Eval pyrolysis (Espitalié et al., 1985). For nitrogen isotopes, 32 samples were selected with TOC values ranging from 1.7% to 24.1%. Content of total nitrogen (N_{tot}) and inorganic nitrogen bound (N_{bnd}) in clay minerals, with their respective isotopic composition ($\delta^{15}N_{tot}$ and $\delta^{15}N_{bnd}$) were determined for each sample following Silva and

Bremner (1966) and Schubert and Calvert (2001). $\delta^{15}N_{org}$ values were calculated by mass balance of $\%N_{bnd}$, $\%N_{tot}$, $\delta^{15}N_{bnd}$ and $\delta^{15}N_{tot}$ (Storme et al., 2012).

Total and inorganic nitrogen content and isotopic composition of samples were determined by isotope-ratio Mass Spectrometry using a Thermo Scientific Delta V plus mass spectrometer connected to a ConFlo IV dilution system, coupled with a Flash 2000 analyzer for elemental analyses. The analytical accuracy and precision of the system were monitored using tyrosine ($\delta^{15}N$ = 10.01‰) as internal laboratory standard, that was calibrated on international standards IAEA-N1 ($\delta^{15}N$ = 0.3‰), IAEA-N2 ($\delta^{15}N$ = 20.1‰) and IAEA-N3 ($\delta^{15}N$ = 4.5‰), with an overall precision better than 0.3‰ above 40 µg of nitrogen and 0.6‰ below this amount. Replicate analyses were performed, with a mean standard deviation better than 0.002% for the nitrogen content and better than 0.2‰ for $\delta^{15}N$ values.

Results

Mineralogy

The mineralogy of rock samples mainly consisted in quartz (0–90%), clays (10–90%), and framboidal pyrite (0–10%). Clay fraction (<2µm) was mainly dominated by kaolinite (0–100%, 65% on average), illite (0–100%, 20% on average) and smectite (0–80%, 15% on average).

A major mineralogical and organic change was recorded at the EOT (Figure 3). The Eocene assemblage was characterized by moderate quartz proportions (0–70%, 30% on average), high kaolinite content among clay minerals (10-100%, 90% on average) and high organic content with TOC values up to 27% (5% on average). In contrast, the Oligocene sediments showed higher quartz content (5–80%, 40% on average) and the appearance of smectite among clay minerals (0–80%, 30% on average), associated with lower kaolinite content (0–100%, 55% on average) and lower TOC values (3% on average).

Remarkably, the proportion of quartz exhibited long-term cyclic-like variations, especially in the Oligocene, with wave length of ~50 m. Similar features were recorded in TOC values, associated with a general decrease of TOC values from the base toward the top of the core.

Nitrogen isotopes ($\delta^{15}N$)

The $\%N_{tot}$ ranged between 0.03% and 0.7% and the $\%N_{bnd}$ between 0.01% and 0.07%, the organic nitrogen corresponding to 32–95% of the total nitrogen (Table 1). The calculated $\delta^{15}N_{org}$ values ranged from 1.1‰ to 6.3‰, with the strongest variation recorded across the EOT (~4.5‰) and lower values below this limit (2.9 ±1.1‰), than above (4.5 ±1.2‰).

Discussion

Clay minerals and $\delta^{15}N_{org}$ values most likely reflect an environmental signal as burial did not exceed 500 m (Bauer et al., 2010; Bauer et al. accepted). In a HI-OI diagram, most of the samples used for $\delta^{15}N_{org}$ analyses plot in a Type-III organic matter and several in a Mix of Type III and I (Figure 4A). This suggests a major contribution of terrestrial organic matter (Type III) and a relatively low contribution of algal-bacterial and/or autochthonous macrophytes material (Espitalié et al., 1985). To first order, it thus allows the interpretation of $\delta^{15}N_{org}$ values as a terrestrial derived signal.

Long-term paleoclimate evolution

Kaolinite results generally from active hydrolysis and ion leaching by chemical weathering in humid/warm conditions, whereas smectite often results from parent rock alteration in poor drained environment under lower hydrolyzing conditions. Smectite could

also be related to the development of confined hydromorphic soils in the catchment area and/or enhanced seasonality (Chamley, 1989; Wright et al., 2000; Schnyder et al., 2006).

Dominant kaolinite during the Eocene thus suggests enhanced hydrolyzing conditions associated to humid/warm conditions, whereas lower hydrolyzing conditions associated with drier/cooler conditions during the Oligocene (Zachos, 2001; Sheldon, 2009) are confirmed from the strong decrease in kaolinite content and the appearance of smectite (Figure 3). Major mineralogical changes are a common signature of the EOT, as reported from Oregon (Kautz, 2002), the Antarctic Ocean (Ehrmann et al., 1992) or the Tibetan Plateau (Zhang and Guo, 2014), suggesting a transition from chemical weathering to physical erosion at the EOT, which is in good agreement with the mineralogical record in CDB1.

The largest mineralogical change occurred between -202 and -197 m, within the Eocene Oligocene boundary interval (-205 to -195 m; Figure 3). In the same interval, TOC values decreased drastically and remained low in the Oligocene as compared to the Eocene. This further supports more humid/warm conditions during the Eocene that favored (i) vegetation growth in the catchment and on the boarders of the lake, and/or (ii) enhanced preservation of the organic matter by the development of dysoxic/anoxic conditions, whereas those favorable conditions declined during the Oligocene. However, no significant change occurred in the framboidal pyrite content (not shown) – indicative of dysoxic/anoxic conditions – between the Eocene and the Oligocene, suggesting that the development of surrounding and shallow lacustrine-palustrine vegetation was the main factor driving the organic matter accumulation.

Leaching processes induced by humid conditions could also explain the low $\delta^{15}N_{org}$ values recorded prior to the EOT (Figure 3), when interpreted as a terrestrial derived signal, as $\delta^{15}N_{org}$ values are negatively correlated with precipitations (Amundson et al., 2003; Swap et al., 2004; Liu and Wang, 2008, 2010). In humid environments, ecosystem productivity is

enhanced and nutrients are consequently limited, leading to nutrient recycling and closed N-cycle, which limits N loss and associated ^{15}N fractionation. In contrast, the ~6‰ increase of the $\delta^{15}N_{org}$ values across the EOT suggests a ^{15}N-enrichment of the plant/soil system by N loss (e.g. gas emission either by nitrification, denitrification and/or volatilization; Aranibar et al., 2004), resulting from low N-recycling in water-limited and nutrients-enriched environments, associated to the demise of the ecosystem productivity (Handley et al., 1999; Swap et al., 2004; Liu and Wang, 2008). If organic matter is mainly of terrestrial origin, the ecosystem productivity refers to the vegetation development in the catchment area and within the lacustrine-palustrine system. $\delta^{15}N_{org}$ values are thus in agreement with the establishment of drier conditions in the Early Oligocene.

However, organic sources may have influenced $\delta^{15}N_{org}$ values either by *in situ* primary production or N_2-fixing organisms (Hollander et al., 1993; Hodell and Schelske, 1998; Paris et al., 2010). Even though a contribution of algal-bacterial and/or autochthonous macrophytes material is suggested by few relatively high HI values (>300 mg HC/g TOC; Figure 4A), their influence on $\delta^{15}N_{org}$ values is thought to be minimal as HI and $\delta^{15}N_{org}$ values were not correlated (Figure 4B). Thus, a climatic control on $\delta^{15}N_{org}$ values is more likely.

Amundson et al. (2003) also suggested that $\delta^{15}N_{org}$ values are positively correlated with temperatures. To this respect, increasing $\delta^{15}N_{org}$ values across the EOT would have potentially suggested warming conditions. This is not consistent with the global cooling recorded worldwide (Zachos, 2001; Mosbrugger et al., 2005; Bohaty et al., 2012; Wade et al., 2012; Hren et al., 2013) and the local palynomorph associations (Bauer et al., accepted). Thus, we propose that in our case water-availability rather than temperatures is the dominant environmental factor controlling $\delta^{15}N_{org}$ values as suggested by Liu and Wang (2008). Consequently, decreasing temperatures during the EOT were probably associated with drier

conditions.

A stepwise Eocene-Oligocene Transition

In CDB1, $\delta^{15}N_{org}$ values, kaolinite and smectite content show a two-step evolution towards drier conditions designated as step 1 and step 2 (Step 1 from -206 to -195 m; Step 2 from -181 to -176 m) and separated by a plateau (Figure 3). The overall evolution from -206 to -176 m constitutes the EOT in CDB1. Several studies in marine environments described a stepwise EOT of ~300 kyr (Coxall et al., 2005; Bohaty et al., 2012), even extended up to ~800 kyr if including EOT-1, EOT-2, Oi-1 and Oi-1a events (Katz et al., 2008). The Oi-1a event was interpreted as an eustatic lowering induced by ice-volume growth, associated with a ~2 °C cooling. It occurred 500 kyr after the Oi-1 at the C13n/C12r Chron transition, which corresponds to a previous ice-volume growth and ~2 °C cooling (Katz et al., 2008). In CDB1, step 1 and 2 are both marked by a change from organic-rich to massive, organic-poor clay, with additional roots development, either highlighting basin filling or water base-level drops that might correspond to the successive sea-level falls identified in the marine realms between EOT-1 and Oi-1a (Katz et al., 2008). Sea level drops would therefore be a likely mechanism for reduced moisture input that triggered drier conditions in the Early Oligocene. However, the exact timing of those steps is unknown in CDB1 and the estimation of duration remains essential to elaborate close correlations between marine and terrestrial records.

Short-term paleoclimate evolution

Unlike the clay assemblages, $\delta^{15}N_{org}$ values were highly variable prior to the EOT. It is probably because the N-cycle reacts faster to local environmental changes (e. g. Andersson et al., 2012) than clay minerals that suppose a long lasting modification of landscapes by major changes in hydrolysis conditions. $\delta^{15}N_{org}$ values increased from 2.0 ±0.7‰ during the

Bartonian/Earliest Priabonian to 4.1 ±1.1‰ in the late Early Priabonian (Figure 3), suggesting drier conditions, in agreement with palynomorph assemblages that stated the disappearance of tropical taxa since the Late Bartonian (Bauer et al., accepted). The positive excursion of the $\delta^{15}N_{org}$ in the late Early Priabonian is associated with a low organic matter accumulation interval, suggesting diminished vegetation cover in the catchment and decreasing lacustrine-palustrine productivity. Among several cooler/drier episodes identified during the Late Eocene (Cavagnetto and Anadón, 1996; Vonhof et al., 2000; Katz et al., 2008), a regional aridification of global significance in Asian interior dated as Early Priabonian (Abels et al., 2011) might be linked to the episode identified in CDB1.

A return to relatively more humid conditions is suggested by lower $\delta^{15}N_{org}$ values (2.7 ±0.6‰) recorded in the Late Priabonian, than in the late Early Priabonian (4.1 ±1.1‰) until the largest shift at the Eocene-Oligocene boundary (Figure 3). Those conditions were probably more suitable for organic matter accumulation in the lacustrine-palustrine system, as recorded by an organic-rich interval in the Late-Priabonian.

In the Early Rupelian, associated with the highest $\delta^{15}N_{org}$ values, the decrease in kaolinite content and the appearance of smectite-rich sediments point to drier/cooler conditions (Figure 3). Such conditions are supported by the development of xerophytic-like plants, which are adapted to dry conditions (Bauer et al., accepted). Despite the low sampling resolution, the alternating negative/positive excursions recorded by the $\delta^{15}N_{org}$ suggests humid/dry cycles (e. g. Storme et al., 2012) and points to unstable climatic conditions as compared to the Eocene. Humid/dry cycles are also supported by (i) the high variation of kaolinite, negatively correlated with smectite, and (ii) the cyclic-like pulses of siliciclastic sediments (recorded by quartz content), which were probably favored by enhanced erosion in a context of decreasing water-base level (Miller et al., 2008) and episodically accelerated water cycle. The cyclic-like detrital input, associated with pulses of TOC, suggests a climatic

control (astronomical?) with the development of organic productivity in the catchment of the lacustrine-palustrine system during moderately more humid/warmer intervals, albeit occurring in a globally cooling/drying general trend.

The unstable climate of the Early Rupelian was probably associated with enhanced seasonality as the formation of smectite is favored under contrasted season climate (Chamley, 1989; Wright et al., 2000). This is confirmed by the disappearance of warm forms pollens and an increase in Herbaceae and Coniferales fractions consecutive to the establishment of a dry season (Bauer et al., accepted). Enhanced seasonality seems to be a widespread characteristic of the Early Oligocene climate as it has already been suggested in Central and Northern Europe (Mosbrugger et al., 2005; Hren et al., 2013), South UK (Gale et al., 2006), northern high latitudes (Eldrett et al., 2009) and America (Ivany et al., 2000; Wade et al., 2012)

Conclusion

The CDB1 core constitutes a rare succession of high resolution, well-preserved terrestrial record that encompasses the EOT. A major mineralogical change and a drastic increase of $\delta^{15}N_{org}$ values occurred at the EOT indicating the transition from warm/humid conditions in the Eocene to cooler/drier conditions in the Oligocene. This transition is stepwise and might record the paleoclimatic events identified in the marine environment between EOT-1 and Oi-1a.

The initiation of the climatic degradation was recorded during the late Early Priabonian (prior to the EOT). During the Early Rupelian, long-lasting humid/dry cycles, associated to enhanced seasonality are suggested as previously reported in both marine and terrestrial environments worldwide. Paleoproductivity patterns in the catchment of the lacustrine-palustrine system fit well with the climatic changes, enhanced vegetation cover being in tune with warmer/more humid conditions.

However, the exact duration of the recorded events remains unknown, although it is essential to elaborate close correlations between marine and terrestrial environments.

Acknowledgments

We are grateful to the CINERGY project and team (BRGM and Rennes 1 University) which provided the material for this study. The financial support for the CDB1 drilling came from local and regional authorities (CG35, Région Bretagne, Métropole Rennes, Chartres-de-Bretagne city council), national contributors (Ademe, AELB, Préfecture de Bretagne) and water resource agencies (IAV, SMPBR, SMG35). G. Rochez is particularly acknowledged for technical support.

See supplementary data for clay minerals and associated TOC values.

References

Abels, H.A., Dupont-Nivet, G., Xiao, G., Bosboom, R., Krijgsman, W., 2011. Step-wise change of Asian interior climate preceding the Eocene–Oligocene Transition (EOT). *Palaeogeogr. Palaeoclimatol. Palaeoecol.*, **299**, 399–412.

Amundson, R., Austin, A.T., Schuur, E. a. G., Yoo, K., Matzek, V., Kendall, C., Uebersax, A., Brenner, D., Baisden, W.T., 2003. Global patterns of the isotopic composition of soil and plant nitrogen. *Glob. Biogeochem. Cycles,* **17**, 1-10.

Andersson, R.A., Meyers, P., Hornibrook, E., Kuhry, P., Mörth, C.-M., 2012. Elemental and isotopic carbon and nitrogen records of organic matter accumulation in a Holocene permafrost peat sequence in the East European Russian Arctic. *J. Quat. Sci.,* **27**, 545-552.

Aranibar, J.N., Otter, L., Macko, S.A., Feral, C.J.W., Epstein, H.E., Dowty, P.R., Eckardt, F., Shugart, H.H., Swap, R.J., 2004. Nitrogen cycling in the soil–plant system along a precipitation gradient in the Kalahari sands. *Glob. Change Biol.*, **10**, 359–373.

Bauer, H., Saint-Marc, P., Bessin, P., Chateauneuf, J.J.C., Bourdillon, C., Wyns, R., Guillocheau, F., accepted. The Cenozoic history of the Armorican Massif: new insights from the deep CDB1 borehole (Rennes Basin, France). *CR Geosci.*

Bauer, H., Wyns, R., Leclercq, M., Palvadeau, E., Guillocheau, F., 2010. CINERGY: Un forage profond dans le bassin de Rennes. *Bull. Inf. Géologues Bassin Paris,* **47**, 3–6.

Bergerat, F., 1987. Stress fields in the European platform at the time of Africa-Eurasia collision. *Tectonics* **6**, 99–132.

Bohaty, S.M., Zachos, J.C., Delaney, M.L., 2012. Foraminiferal Mg/Ca evidence for Southern Ocean cooling across the Eocene–Oligocene transition. *Earth Planet. Sci. Lett.* **317–318**, 251–261.

Cavagnetto, C., Anadón, P., 1996. Preliminary palynological data on floristic and climatic changes during the Middle Eocene-Early Oligocene of the eastern Ebro Basin, northeast Spain. *Rev. Palaeobot. Palynol.* **92**, 281–305.

Chamley, H., 1989. *Clay Sedimentology*, Springer Verlag.

Coxall, H.K., Wilson, P.A., Pälike, H., Lear, C.H., Backman, J., 2005. Rapid stepwise onset of Antarctic glaciation and deeper calcite compensation in the Pacific Ocean. *Nature,* **433**, 53–57.

Dera, G., Pellenard, P., Neige, P., Deconinck, J.-F., Pucéat, E., Dommergues, J.-L., 2009. Distribution of clay minerals in Early Jurassic Peritethyan seas: Palaeoclimatic significance inferred from multiproxy comparisons. *Palaeogeogr. Palaeoclimatol. Palaeoecol.,* **271**, 39–51.

Dèzes, P., Schmid, S.M., Ziegler, P.A., 2004. Evolution of the European Cenozoic Rift System: interaction of the Alpine and Pyrenean orogens with their foreland lithosphere. *Tectonophysics*, **389**, 1–33.

Dupont-Nivet, G., Krijgsman, W., Langereis, C.G., Abels, H.A., Dai, S., Fang, X., 2007. Tibetan plateau aridification linked to global cooling at the Eocene–Oligocene transition. *Nature,* **445**, 635–638.

Ehrmann, W.U., Melles, M., Kuhn, G., Grobe, H., 1992. Significance of clay mineral assemblages in the Antarctic Ocean. *Mar. Geol.*, **107**, 249–273.

Eldrett, J.S., Greenwood, D.R., Harding, I.C., Huber, M., 2009. Increased seasonality through the Eocene to Oligocene transition in northern high latitudes. *Nature,* **459**, 969–973.

Espitalié, J., Deroo, D., Marquis, F., 1985. La pyrolise Rock-Eval et ses applications. Revue de l'Institut Français du Pétrole, 563–579, 755–784.

Esteoule-Choux, J., Bos, P., Blanchet, C., 1988. Le bassin tertiaire de Pipriac (Ille-et-Vilaine) : Structure, mise en évidence de dépôts oligocènes. *Géologie Fr.*, **1**, 47–50.

Gale, A.S., Huggett, J.M., PÄlike, H., Laurie, E., Hailwood, E.A., Hardenbol, J., 2006. Correlation of Eocene–Oligocene marine and continental records: orbital cyclicity, magnetostratigraphy and sequence stratigraphy of the Solent Group, Isle of Wight, UK. *J. Geol. Soc.*, **163**, 401–415.

Handley, L.L., Austin, A.T., Stewart, G.R., Robinson, D., Scrimgeour, C.M., Raven, J.A., Heaton, T.H.E., Schmidt, S., 1999. The ^{15}N natural abundance ($\delta^{15}N$) of ecosystem samples reflects measures of water availability. *Funct. Plant Biol.*, **26**, 185–199.

Hodell, D.A., Schelske, C.L., 1998. Production, sedimentation, and isotopic composition of organic matter in Lake Ontario. *Limnol. Oceanogr.*, **43**, 200–214.

Hollander, D.J., Sinninghe Damsté, J.S., Hayes, J.M., de Leeuw, J.W., Huc, A.Y., 1993. Molecular and bulk isotopic analyses of organic matter in marls of the Mulhouse Basin (Tertiary, Alsace, France). *Org. Geochem.*, **20**, 1253–1263.

Hren, M.T., Sheldon, N.D., Grimes, S.T., Collinson, M.E., Hooker, J.J., Bugler, M., Lohmann, K.C., 2013. Terrestrial cooling in Northern Europe during the eocene-oligocene transition. *Proc. Natl. Acad. Sci. U. S. A.*, **110**, 7562–7567.

Ivany, L.C., Patterson, W.P., Lohmann, K.C., 2000. Cooler winters as a possible cause of mass extinctions at the Eocene/Oligocene boundary. *Nature*, **407**, 887–890.

Jaeger, J.L., 1967. Un alignement d'anomalies légères coïncidant avec des bassins tertiaires en Bretagne. *Mém. BRGM No. 52.*

Katz, M.E., Miller, K.G., Wright, J.D., Wade, B.S., Browning, J.V., Cramer, B.S., Rosenthal, Y., 2008. Stepwise transition from the Eocene greenhouse to the Oligocene icehouse. *Nat. Geosci.*, **1**, 329–334.

Kautz, C.Q., 2002. The mineralogical record of Eocene-Oligocene climate change in the Clarno and John Day Formations, central Oregon [WWW Document]. URL https://www.researchgate.net

Kennett, J.P., Shackleton, N.J., 1976. Oxygen isotopic evidence for the development of the psychrosphere 38 Myr ago. *Nature*, **260**, 513–515.

Lear, C.H., Bailey, T.R., Pearson, P.N., Coxall, H.K., Rosenthal, Y., 2008. Cooling and ice growth across the Eocene-Oligocene transition. *Geology*, **36**, 251–254.

Liu, W., Wang, Z., 2008. Nitrogen isotopic composition of plant-soil in the Loess Plateau and its responding to environmental change. *Chin. Sci. Bull.*, **54**, 272–279.

Liu, X., Wang, G., 2010. Measurements of nitrogen isotope composition of plants and surface soils along the altitudinal transect of the eastern slope of Mount Gongga in southwest China. R*apid Commun. Mass Spectrom.*, **24**, 3063–3071.

Meunlenkamp, J.E., Sissingh, W., Popov, S.V., Kovac, M., Bergerat, F., 2010. Paleogeographic map of Late Rupelian. In: *Atlas peri-Tethys palaeogeographical maps* (Ed. by Dercourt, J., Gaetani, M., Vrielynck, B., Barrier, E., Biju-Duval, B., Brunet, M.F., Cadet, J.P., Crasquin, S. and Sandulescu, M.) Peri-Thetys Programme, 1 map.

Miller, K.G., Browning, J.V., Aubry, M.-P., Wade, B.S., Katz, M.E., Kulpecz, A.A., Wright, J.D., 2008. Eocene–Oligocene global climate and sea-level changes: St. Stephens Quarry, Alabama. *Geol. Soc. Am. Bull.*, **120**, 34–53.

Moore, D.M., Reynolds, R.C.J., 1997. X-Ray Diffraction and the Identification and Analysis of Clay Mineral.

Mosbrugger, V., Utescher, T., Dilcher, D.L., 2005. Cenozoic continental climatic evolution of Central Europe. *Proc. Natl. Acad. Sci. U. S. A.*, **102**, 14964–14969.

Ollivier-Pierre, M.-F., Gruas-Cavagnetto, C., Roche, E., Schuler, M., 1987. Eléments de flore de type tropical et variations climatiques au Paléogène dans quelques bassins d'Europe Nord-Occidentale. In: *Mémoires et travaux de l'Institut de Montpellier.* **17**, 173–205.

Ollivier-Pierre, M.F., Maupin, C., Estéoule-Choux, J., Sittler, C., 1993. Transgression et paleoenvironnement à l'Oligocène en Bretagne (France). Sédimentologie, micropaléontologie, palynologie et palynofaciès du Rupélien du Bassin de Rennes. *Palaeogeogr. Palaeoclimatol. Palaeoecol.*, **103**, 223–250.

Paris, G., Beaumont, V., Bartolini, A., Clémence, M.-E., Gardin, S., Page, K., 2010. Nitrogen isotope record of a perturbed paleoecosystem in the aftermath of the end-Triassic crisis, Doniford section, SW England. *Geochem. Geophys. Geosystems* **11**(8).

Schnyder, J., Ruffell, A., Deconinck, J.-F., Baudin, F., 2006. Conjunctive use of spectral gamma-ray logs and clay mineralogy in defining late Jurassic–early Cretaceous

palaeoclimate change (Dorset, U.K.). *Palaeogeogr. Palaeoclimatol. Palaeoecol.*, **229**, 303–320.

Schubert, C.J., Calvert, S.E., 2001. Nitrogen and carbon isotopic composition of marine and terrestrial organic matter in Arctic Ocean sediments: implications for nutrient utilization and organic matter composition. *Deep Sea Res. Part Oceanogr. Res. Pap.,* **48**, 789–810.

Sheldon, N.D., 2009. Nonmarine records of climatic change across the Eocene-Oligocene transition. *Geol. Soc. Am. Spec. Pap.,* **452**, 241–248.

Silva, J.A., Bremner, J.M., 1966. Determination and Isotope-Ratio Analysis of Different Forms of Nitrogen in Soils: 5. Fixed Ammonium. *Soil Sci. Soc. Am. J.* **30**, 587–594.

Storme, J.-Y., Dupuis, C., Schnyder, J., Quesnel, F., Garel, S., Iakovleva, A.I., Iacumin, P., Di Matteo, A., Sebilo, M., Yans, J., 2012. Cycles of humid-dry climate conditions around the P/E boundary: new stable isotope data from terrestrial organic matter in Vasterival section (NW France). *Terra Nova*, **24**, 114–122.

Swap, R.J., Aranibar, J.N., Dowty, P.R., Gilhooly III, W.P., Macko, S.A., 2004. Natural abundance of ^{13}C and ^{15}N in C_3 and C_4 vegetation of southern Africa: patterns and implications. *Glob. Change Biol.*, **10**, 350–358.

Thomas, E., 1999. Evolution Cénozoïque d'un domaine de socle: Le massif Armoricain. Unpubl. doctoral dissertation, Université de Rennes 1, France.

Vonhof, H.B., Smit, J., Brinkhuis, H., Montanari, A., Nederbragt, A.J., 2000. Global cooling accelerated by early late Eocene impacts? *Geology*, **28**, 687–690.

Wade, B.S., Houben, A.J.P., Quaijtaal, W., Schouten, S., Rosenthal, Y., Miller, K.G., Katz, M.E., Wright, J.D., Brinkhuis, H., 2012. Multiproxy record of abrupt sea-surface cooling across the Eocene-Oligocene transition in the Gulf of Mexico. *Geology*, **40**, 159–162.

Wright, V.P., Taylor, K.G., Beck, V.H., 2000. The Paleohydrology of Lower Cretaceous Seasonal Wetlands, Isle of Wight, Southern England. *J. Sediment. Res.*, **70**, 619–632.

Zachos, J., 2001. Trends, Rhythms, and Aberrations in Global Climate 65 Ma to Present. *Science*, **292**, 686–693.

Zhang, C., Guo, Z., 2014. Clay mineral changes across the Eocene–Oligocene transition in the sedimentary sequence at Xining occurred prior to global cooling. *Palaeogeogr. Palaeoclimatol. Palaeoecol.*, **411**, 18–29.

Figure Captions

Table 1: Organic geochemistry of the CDB1 core. HI, Hydrogen Index (mg HC/g TOC); OI, Oxygen Index (mg CO_2/g TOC); TOC, Total Organic Carbon; TN, Total Nitrogen; N_{bnd}, Nitrogen bound in clay minerals that remained after KOBr-KOH treatment; N_{org}, organic nitrogen; FrN_{org}, the per cent organic nitrogen of the total nitrogen in a sample; $\Delta^{15}N_{tot}$ and $\Delta^{15}N_{bnd}$, error on the $\delta^{15}N_{tot}$ and $\delta^{15}N_{bnd}$ values (isotopic values of N_{tot} and N_{bnd}), respectively, based on the standard deviation of the isotopic values calculated with at least two replicates. ([1]) Samples measured on low nitrogen amount (<40µg), the highest mean standard deviation was applied, based on tyrosines (internal laboratory standard) measured on similar amount (5 to 40µg; n=46) of nitrogen in 9 series. ([2]) No available replicates for this sample, the mean standard deviation calculated on tyrosines (>40 µg; n=87) was applied. ([3]) Simplified combining error of the $\delta^{15}N_{org}$ estimated with negligible errors on nitrogen contents following $\Delta^{15}N_{org} = \Delta^{15}N_{tot} + \Delta^{15}N_{bnd} (1 - FrN_{org}/100)$.

Figure 1: Geological map of the Rennes Basin showing the Cenozoic formations and the position of the CDB1 borehole modified from Thomas (1999). Simplified paleogeography of the Late Rupelian is also represented (Meunlenkamp et al., 2010)

Figure 2: Lithostratigraphy, age limits and palynological data of CDB1 from Bauer et al. 2010 and Bauer et al. accepted. E/O, Eocene Oligocene boundary between -205 and -195 m, based on palynomorphs association and magnetostratigraphy (Bauer et al., accepted; Boulila et al., unpublished).

Figure 3: High-resolution mineralogy and organic geochemistry of CDB1. The grey line and its envelope represent the $\delta^{15}N_{org}$ and its associated error (see Table 1). The $\delta^{15}N_{tot}$ (black line) is clearly driven by the $\delta^{15}N_{org}$. Blue zones highlight periods of increased humidity. Step 1*, EOT 1 + EOT 2 + Oi-1? Barton. for Bartonian. E. Priab. Event might refers to the Asian regional aridification identified in Abels et al. 2011. Black stars correspond to samples with HI>300 mg CO_2/g TOC, suggesting algal influence. Age limits were based on Bauer et al. (2010) and Bauer et al. (accepted).

Figure 4: A, HI-OI diagram and B, $\delta^{15}N_{org}$ vs HI values, showing no correlation between $\delta^{15}N_{org}$ and high (black points) or low HI (grey points) values. High HI values suggest an algal-bacterial and/or macrophytes influence.

Samples	Position (m)	HI	OI	TOC (%)	TN (%)	N_{bnd} (%)	N_{org} (%)	FrN_{org} (%)	$\delta\ ^{15}N_{tot}$ (‰)	$\Delta^{15}N_{tot}$ (1σ)	$\delta\ ^{15}N_{bnd}$ (‰)	$\Delta^{15}N_{bnd}$ (1σ)	$\delta\ ^{15}N_{org}$ (‰)	$\Delta^{15}N_{org}$[3] (1σ)
CDB1-585	91.4	279	57	5.0	0.15	0.04	0.11	73	5.7	0.04	5.9	0.60[1]	5.6	0.20
CDB1-605	101.9	156	31	4.7	0.05	0.03	0.02	32	4.5	0.60[1]	5.2	0.60[1]	3.1	1.01
CDB1-662	128.2	274	50	3.9	0.14	0.05	0.09	64	5.8	0.06	5.4	0.60[1]	6.0	0.28
CDB1-060	134.9	-	-	4.4	0.12	0.05	0.07	59	4.8	0.17	5.3	0.60[1]	4.5	0.42
CDB1-682	138.8	41	120	8.2	0.09	0.03	0.06	66	3.4	0.07	5.2	0.60[1]	2.4	0.28
CDB1-692	144.0	83	69	3.3	0.13	0.03	0.10	78	3.6	0.14	4.9	0.60[1]	3.2	0.27
CDB1-1326	176.1	212	44	4.5	0.18	0.04	0.14	77	6.3	0.25	6.1	0.60[1]	6.3	0.39
CDB1-1324	178.4	134	42	2.6	0.08	0.03	0.05	57	5.3	0.60[1]	5.8	0.60[1]	5.0	0.86
CDB1-1320	181.3	168	60	8.2	0.37	0.04	0.33	88	5.1	0.06	5.3	0.60[1]	5.0	0.13
CDB1-791	184.1	314	64	11.8	0.19	0.04	0.15	79	4.9	0.01	6.0	0.60[1]	4.6	0.13
CDB1-092	187.5	230	45	3.7	0.13	0.04	0.10	73	5.0	0.14	5.8	0.60[1]	4.7	0.30
CDB1-1304	195.2	164	59	3.2	0.10	0.03	0.07	69	4.6	0.16	6.1	0.60[1]	3.9	0.35
CDB1-839	206.0	116	27	4.9	0.13	0.02	0.11	82	2.0	0.02	4.2	0.60[1]	1.5	0.13
CDB1-106	208.9	-	-	7.0	0.27	0.04	0.23	87	2.9	0.11	4.8	0.60[1]	2.6	0.19
CDB1-857	213.9	418	61	24.1	0.69	0.07	0.61	90	3.4	0.04	5.4	0.60[1]	3.2	0.10
CDB1-121	219.3	31	51	6.8	0.25	0.03	0.22	87	3.1	0.04	5.5	0.60[1]	2.7	0.12
CDB1-871	222.4	99	79	6.4	0.21	0.03	0.18	84	2.6	0.11	5.2	0.60[1]	2.1	0.21
CDB1-875	225.2	107	88	8.8	0.21	0.04	0.17	82	2.8	0.09	4.2	0.60[1]	2.5	0.19
CDB1-1276	228.4	317	42	8.1	0.24	0.03	0.21	87	3.3	0.07	4.8	0.60[1]	3.0	0.15
CDB1-1262	239.0	79	89	10.9	0.34	0.03	0.31	91	3.2	0.08	4.4	0.60[1]	3.1	0.13
CDB1-1260	241.0	98	84	8.2	0.26	0.03	0.23	90	2.5	0.10	4.4	0.60[1]	2.3	0.16
CDB1-1248	249.7	311	64	8.8	0.26	0.01	0.24	95	3.5	0.07	4.8	0.60[1]	3.4	0.09
CDB1-952	264.7	32	99	1.8	0.08	0.02	0.06	79	3.7	0.03	5.5	0.60[1]	3.3	0.16
CDB1-158	275.7	241	22	6.9	0.26	0.03	0.23	87	4.8	0.17	6.2	0.60[1]	4.6	0.25
CDB1-986	280.6	45	84	4.1	0.14	0.04	0.10	73	2.8	0.04	4.6	0.60[1]	2.2	0.21
CDB1-1008	290.2	386	25	3.3	0.10	0.02	0.08	82	4.7	0.31	4.7	0.60[1]	4.7	0.42
CDB1-1192	295.2	48	79	1.7	0.07	0.02	0.05	72	4.7	0.60[1]	5.7	0.60[1]	4.3	0.77
CDB1-1037	307.9	30	38	2.3	0.03	0.01	0.02	57	5.4	0.60[1]	6.0	0.60[1]	5.0	0.86
CDB1-1059	326.0	44	84	2.4	0.09	0.02	0.07	75	2.1	0.30[2]	5.4	0.60[1]	1.1	0.45
CDB1-1080	337.0	455	34	18.6	0.39	0.02	0.37	94	2.9	0.06	5.2	0.89	2.8	0.11
CDB1-232	358.3	271	49	13.1	0.32	0.05	0.27	84	2.7	0.08	4.3	0.60[1]	2.4	0.17
CDB1-1134	380.6	155	53	3.7	0.11	0.02	0.09	81	2.5	0.19	4.8	0.60[1]	1.9	0.30
	Average			**6.7**	**0.19**	**0.03**	**0.16**	**77**	**2.9**		**5.2**		**3.5**	

Table 1

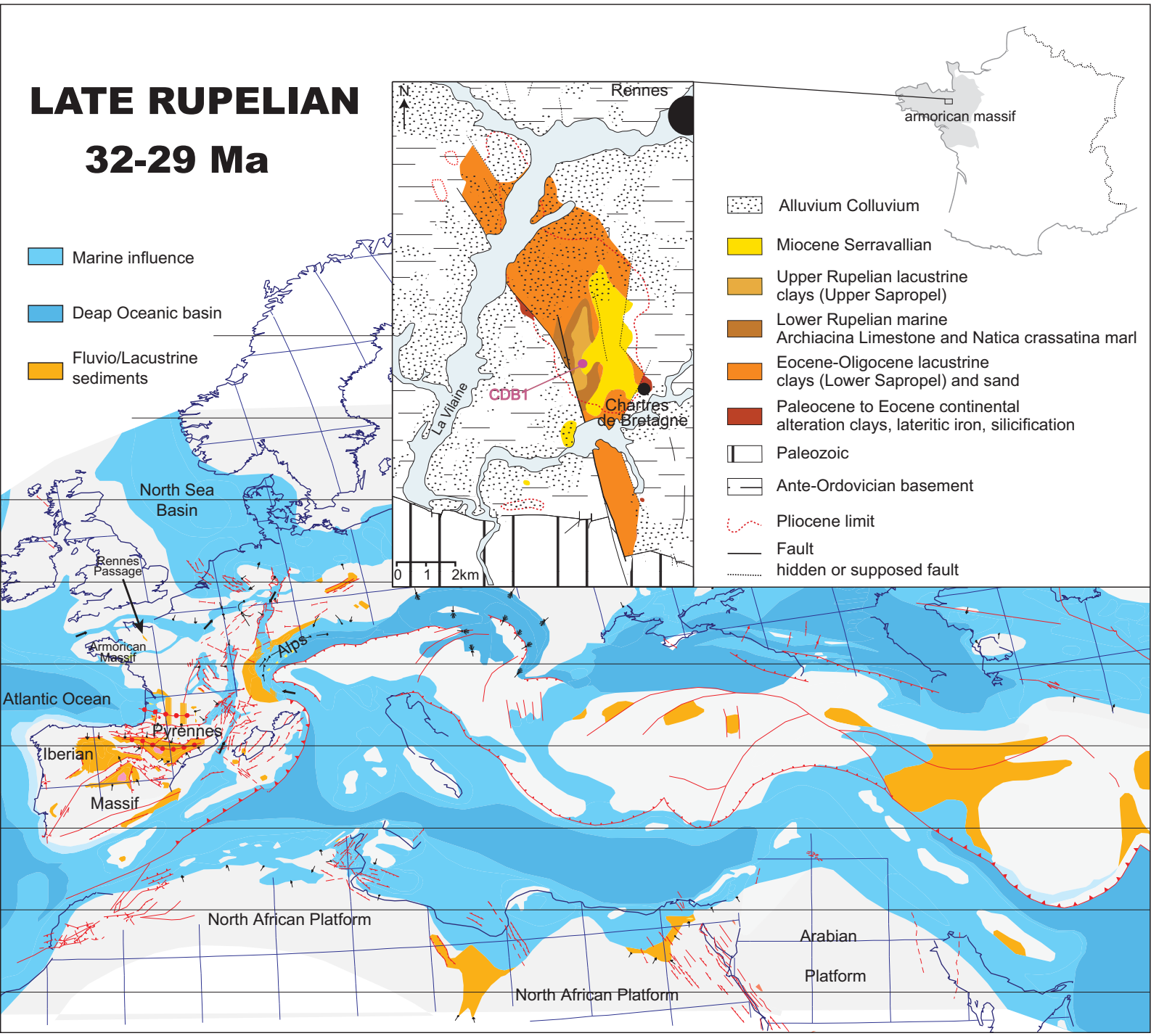
LATE RUPELIAN
32-29 Ma
Marine influence
Deap Oceanic basin
Fluvio/Lacustrine sediments
North Sea Basin
Rennes Passage
Armorican Massif
Atlantic Ocean
Alps
Pyrennes
Iberian
Massif
North African Platform
North African Platform
Arabian
Platform
N
Rennes
La Vilaine
CDB1
Chartres de Bretagne
0 1 2km
armorican massif
Alluvium Colluvium
Miocene Serravallian
Upper Rupelian lacustrine clays (Upper Sapropel)
Lower Rupelian marine Archiacina Limestone and Natica crassatina marl
Eocene-Oligocene lacustrine clays (Lower Sapropel) and sand
Paleocene to Eocene continental alteration clays, lateritic iron, silicification
Paleozoic
Ante-Ordovician basement
Pliocene limit
Fault
hidden or supposed fault

Figure 1

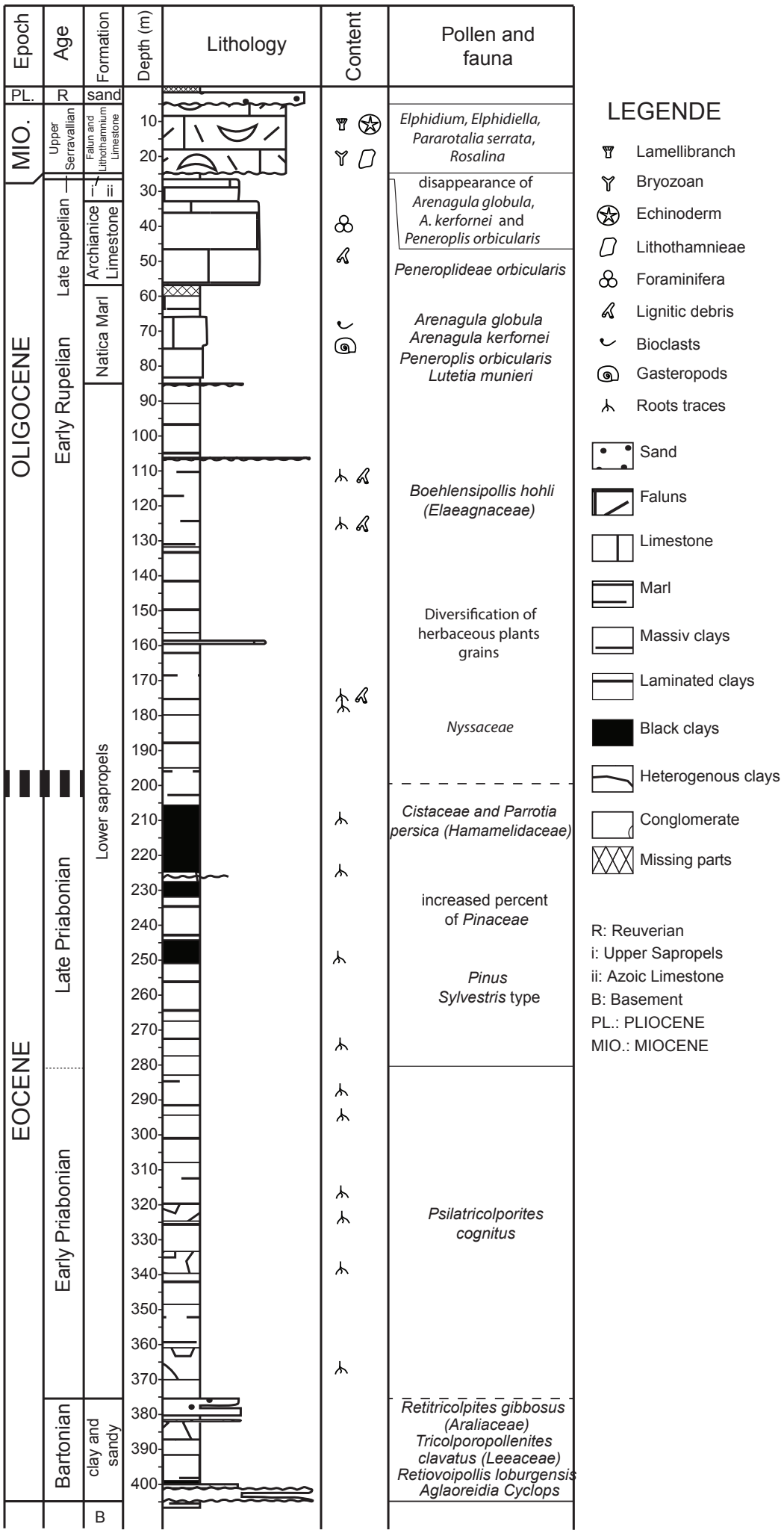
Epoch
Age
Formation
Depth (m)
Lithology
Content
Pollen and fauna
PL.
R
sand
MIO.
Upper Serravallian
Falun and Lithothamnium Limestone
i
ii
OLIGOCENE
Late Rupelian
Archianice Limestone
Early Rupelian
Natica Marl
Lower sapropels
EOCENE
Late Priabonian
Early Priabonian
Bartonian
clay and sandy
B
10
20
30
40
50
60
70
80
90
100
110
120
130
140
150
160
170
180
190
200
210
220
230
240
250
260
270
280
290
300
310
320
330
340
350
360
370
380
390
400
Elphidium, Elphidiella, Pararotalia serrata, Rosalina
disappearance of Arenagula globula, A. kerfornei and Peneroplis orbicularis
Peneroplideae orbicularis
Arenagula globula
Arenagula kerfornei
Peneroplis orbicularis
Lutetia munieri
Boehlensipollis hohli (Elaeagnaceae)
Diversification of herbaceous plants grains
Nyssaceae
Cistaceae and Parrotia persica (Hamamelidaceae)
increased percent of Pinaceae
Pinus Sylvestris type
Psilatricolporites cognitus
Retitricolpites gibbosus (Araliaceae)
Tricolporopollenites clavatus (Leeaceae)
Retiovoipollis loburgensis
Aglaoreidia Cyclops
LEGENDE
Lamellibranch
Bryozoan
Echinoderm
Lithothamnieae
Foraminifera
Lignitic debris
Bioclasts
Gasteropods
Roots traces
Sand
Faluns
Limestone
Marl
Massiv clays
Laminated clays
Black clays
Heterogenous clays
Conglomerate
Missing parts
R: Reuverian
i: Upper Sapropels
ii: Azoic Limestone
B: Basement
PL.: PLIOCENE
MIO.: MIOCENE

Figure 2

Climates
Isotopes
Rock-Eval Pyr.
Bulk XRD
Clay fraction XRD
Lithology
Depth (m)
Age
Epoch
Oligocene
Eocene
E/O
Early Rupelian
Late Priabonian
Early Priabonian
Barton.
100
150
200
250
300
350
400
% Smectite
% Kaolinite
% Quartz
% TOC
δ15N values (‰, VS-N2AIR)
Step 2 (Oi-1a ?)
Plateau
Step 1*
EOT
E. Priab. Event ?
δ15Norg
δ15Ntot
More humid
?
Warm/Humid
Cooler/Drier
warmest/most humid
drier/cooler
warm/humid
humid/dry cycles ?

Figure 3

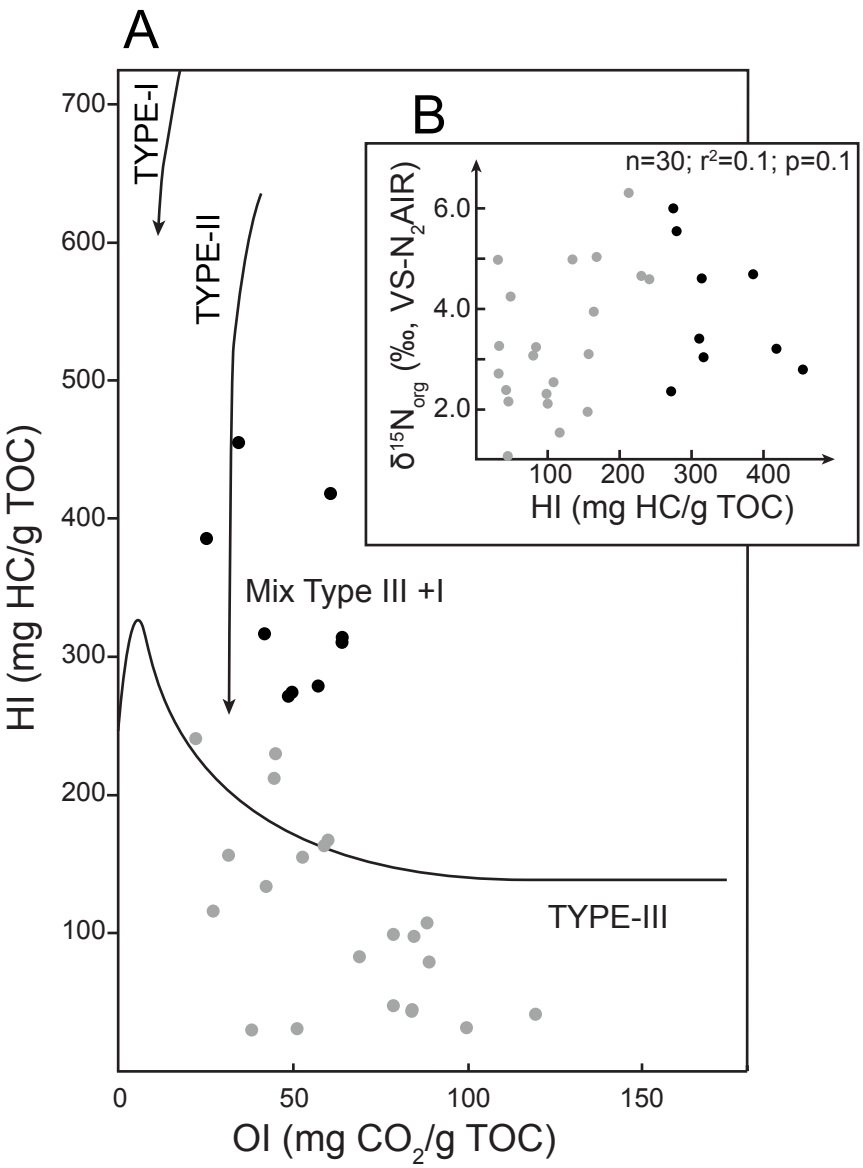
A
B
TYPE-I
TYPE-II
Mix Type III +I
TYPE-III
HI (mg HC/g TOC)
OI (mg CO2/g TOC)
0
50
100
150
100
200
300
400
500
600
700
n=30; r2=0.1; p=0.1
δ15Norg (‰, VS-N2AIR)
2.0
4.0
6.0
100
200
300
400
HI (mg HC/g TOC)

Figure 4

What follows is supplementary material,

which will be made available online but

will not appear in the print version.

Samples	Position	Quartz	Smectite	Kaolinite	TOC
	(m)	(%)	(%)	(%)	(%)
CDB1-303	405.105	17	0	82	
CDB1-1163	402.415				0.0
CDB1-291	399.78	41	0	87	
CDB1-1155	395.2				0.2
CDB1-281	392.3				4.0
CDB1-497	391.53	22	0	92	
CDB1-1149	390.5				0.1
CDB1-1145	388.1				1.3
CDB1-273	387.03	29	0	87	
CDB1-271	385.975	18	0	89	7.6
CDB1-1141	384.6				7.1
CDB1-269	383.805	15			
CDB1-267	381.4				18.9
CDB1-1135	380.59				3.7
CDB1-265	377.7				0.6
CDB1-261	375.41	21	0	97	
CDB1-257	373.9				0.3
CDB1-253	372.305	4			
CDB1-251	371.79				27.2
CDB1-249	370.925	14	0	95	
CDB1-245	368.58				0.4
CDB1-1125	366.665				0.2
CDB1-1117	363.39				9.0
CDB1-1115	362				3.8
CDB1-241	360.65	26	0	100	
CDB1-1111	360.15				18.4
CDB1-239	359.26	29	0	77	
CDB1-233	358.3				13.1
CDB1-231	357.115	36	4	83	
CDB1-1109	356.2				6.2
CDB1-1107	355.89		0	77	
CDB1-1105	354.7				0.4
CDB1-1101	352.575		0	98	
CDB1-1099	351.6				0.1
CDB1-1097	348.985		0	98	0.2
CDB1-1093	347				1.4
CDB1-1091	345.795		0	96	
CDB1-221	345.27				0.9
CDB1-1089	341.94		0	97	1.6
CDB1-1087	340.8				2.6
CDB1-217	338.62	11	0	61	
CDB1-215	338.04	11	0	100	
CDB1-1083	337.6		0	100	
CDB1-1081	337				18.6
CDB1-1075	334.8				9.7
CDB1-1071	333.2		0	98	
CDB1-1069	332.59				0.8

CDB1-1067	330.195		0	97	3.4
CDB1-1063	328.4				5.9
CDB1-211	327.64	33			
CDB1-1058	326.025		0	96	2.4
CDB1-209	325.295	25	0	52	2.8
CDB1-207	324.35	0	0	75	
CDB1-205	323.25	6	0	96	
CDB1-203	322.42		0	84	
CDB1-203	322.42	8	0	95	
CDB1-199	321.275	15	0	97	4.5
CDB1-1055	320.1		3	93	
CDB1-193	319.41	35	0	97	
CDB1-1053	317.32		0	97	2.2
CDB1-1051	314.6				0.9
CDB1-189	313.975	7	0	100	
CDB1-187	313.85	9	0	98	
CDB1-185	312.65	0			
CDB1-1045	312.115	0	0	100	0.0
CDB1-1043	310.725	0			0.9
CDB1-1041	309.845	28			
CDB1-183	309.19	25			
CDB1-1039	308.105	30	0	98	
CDB1-1037	307.87	34			2.3
CDB1-1035	307.585	44	0	98	
CDB1-179	307.16	41			0.8
CDB1-1032	306.63		0	99	
CDB1-1177	306.13	41			1.2
CDB1-1031	305.67	28	0	98	
CDB1-1179	305.13	40			
CDB1-1029	304.7	35	0	98	0.7
CDB1-1027	304.175	35			
CDB1-1181	303.705	13	0	96	0.9
CDB1-1183	303.28	22			
CDB1-177	302.86	19	0	99	0.7
CDB1-1185	302.3425	23			
CDB1-1025	301.965	31	0	96	0.9
CDB1-1187	301.405	14	0	96	
CDB1-175	300.73	14	0	98	1.0
CDB1-1023	299.995	24			
CDB1-1189	298.825	22	0	99	1.0
CDB1-1021	298.165	14			
CDB1-1019	297.65	13			1.0
CDB1-173	297.09	13			
CDB1-1191	296.19	15	0	96	
CDB1-1017	295.53	38	0	95	1.3
CDB1-1193	295.15	20	0	94	1.7
CDB1-1015	294.665	23			1.2
CDB1-1195	294.015	27	0	94	
CDB1-1013	293.465	24			0.5

CDB1-170	292.71	26	0	93	
CDB1-1197	292.025	25			1.5
CDB1-1011	291.275	32	0	96	
CDB1-1199	290.74	25			2.5
CDB1-1009	290.165	27	0	93	3.3
CDB1-1201	289.775	38			
CDB1-1007	289.3	38			
CDB1-168	288.845	27			0.8
CDB1-1203	288.475	21			
CDB1-1005	288.025	25	0	47	1.9
CDB1-1003	287.525	12			
CDB1-1001	286.37	41	14	77	0.3
CDB1-999	285.725	27			
CDB1-1205	285.3				1.7
CDB1-997	284.865	45	3	92	
CDB1-164	284.345	9			1.3
CDB1-1207	284.015	29			
CDB1-995	283.445	22	0	95	4.8
CDB1-993	283	33			
CDB1-1209	282.52	30			1.1
CDB1-991	281.875	27	0	90	
CDB1-989	281.455	32			1.8
CDB1-1211	281.025	26	0	82	
CDB1-987	280.64	24			4.1
CDB1-1213	280.18	25	0	100	
CDB1-162	279.825	18			8.9
CDB1-1215	279.41	21	0	80	
CDB1-985	279.045	45			5.5
CDB1-1217	278.59	30			
CDB1-983	278.23	29			
CDB1-1047	277.985	30	0	87	
CDB1-981	277.755	37			12.8
CDB1-979	276.79				14.1
CDB1-1221	276.365		20	67	
CDB1-158	275.725	27	0	83	6.9
CDB1-977	275.45	44			
CDB1-155	274.945	22	0	73	
CDB1-975	274.34	31			4.3
CDB1-154	273.15	16	0	92	15.0
CDB1-973	272.51	18			
CDB1-1225	272.14		0	89	1.2
CDB1-971	271.73	41			
CDB1-969	271.275	61	0	100	0.1
CDB1-152	269.65	69			0.0
CDB1-965	269.105	63			
CDB1-963	268.31	30			
CDB1-959	267.57	2			
CDB1-1227	267.075	16	0	52	
CDB1-957	266.51	8			

CDB1-150	265.87	17			
CDB1-955	265.125		0	94	
CDB1-953	264.69	54			1.8
CDB1-148	264.25	35	0	95	
CDB1-951	263.78	47	0	96	
CDB1-1229	263.255	38			0.9
CDB1-949	262.555	30	0	95	
CDB1-947	262.015	54			
CDB1-1231	261.335	54			0.7
CDB1-146	260.685	39			
CDB1-945	259.845	43	0	95	0.6
CDB1-943	259.245	63			
CDB1-1233	258.835	31	0	94	0.8
CDB1-941	258.28	33			
CDB1-1235	257.855	43	0	94	1.0
CDB1-144	257.295	63			
CDB1-1237	256.88	34	0	94	1.0
CDB1-939	256.435	41			
CDB1-1239	255.97	33	0	94	
CDB1-937	255.59	59			1.2
CDB1-1241	255.045	40	0	94	
CDB1-935	254.545	57			1.7
CDB1-1243	254.145	37	0	95	
CDB1-933	253.565	69	0	7	1.5
CDB1-1245	253.165	62			
CDB1-931	252.735	58	0	91	1.5
CDB1-929	251.94	65			
CDB1-1247	251.53	34			7.8
CDB1-927	251.07	52			
CDB1-142	250.52	45			20.6
CDB1-925	250.075	30			
CDB1-1249	249.65	58	0	92	8.8
CDB1-923	249.31	55	0	81	
CDB1-1251	248.805	43			11.9
CDB1-921	248.39	21	0	88	
CDB1-140	247.74	30			27.0
CDB1-919	247.06	15	0	100	
CDB1-138	246.73	10			9.0
CDB1-1253	246.455	11	0	96	
CDB1-917	245.85	10			
CDB1-1255	245.385	12	0	92	1.6
CDB1-913	244.82	9			
CDB1-136	244.29	13	0	97	23.6
CDB1-911	243.84	34			
CDB1-1257	243.465	27	0	95	
CDB1-909	242.985	31			10.6
CDB1-1259	242.575	20			
CDB1-907	242.105	31	0	96	9.6
CDB1-905	241.52	27			

CDB1-1261	241.045	29	0	92	8.2
CDB1-903	240.6	28	0	93	
CDB1-134	239.85	30			7.9
CDB1-901	239.435	31			
CDB1-1263	239	10	0	94	10.9
CDB1-899	238.61	28			
CDB1-1265	238.1	22	0	93	8.4
CDB1-897	237.535	38			
CDB1-1267	236.985	8	0	95	4.4
CDB1-895	236.58	42			
CDB1-893	235.85	23	0	95	2.7
CDB1-891	235.115	28			
CDB1-889	234.545	30	0	92	1.9
CDB1-132	234	23			
CDB1-1269	233.435	14	0	92	3.2
CDB1-887	232.89	38			
CDB1-1271	232.525	9	0	68	1.9
CDB1-131	232.07	39			
CDB1-885	231.38	15	0	93	23.7
CDB1-1273	230.235	14	0	89	12.7
CDB1-129	229.66	22	0	94	
CDB1-1275	229.065	12			15.3
CDB1-1277	228.435	19			8.1
CDB1-127	227.165	15	0	93	
CDB1-881	226.825	21			1.4
CDB1-879	226.085	30	0	88	
CDB1-877	225.685	23			
CDB1-875	225.15	23	0	93	8.8
CDB1-873	224.64	25	0	88	
CDB1-1279	224.295	19	0	94	5.3
CDB1-125	223.49	35	0	92	
CDB1-1281	223.375	34			
CDB1-871	222.4	24	0	94	6.4
CDB1-123	221.935	31			
CDB1-1283	221.125	34	0	94	6.9
CDB1-869	220.605	29			
CDB1-867	219.955	10			
CDB1-121	219.275	26	0	95	6.8
CDB1-865	218.945	24			
CDB1-1285	218.525	37	0	89	
CDB1-119	217.955	22			
CDB1-863	217.555	25			3.8
CDB1-1287	216.935	29			
CDB1-116	216.365	36	0	93	4.8
CDB1-114	216.255	38			
CDB1-861	215.635	32	0	87	
CDB1-1289	214.975	32			4.9
CDB1-859	214.45	48			
CDB1-857	213.85	22	0	89	24.1

CDB1-113	213.58	17	0	94	
CDB1-855	212.97	44			
CDB1-1291	211.64	18			7.7
CDB1-853	211.01	27	0	94	8.0
CDB1-1293	210.67	11	3	92	2.7
CDB1-109	209.995	24	0	95	
CDB1-851	209.625	25	0	97	4.5
CDB1-1295	209.47	18			
CDB1-849	209.135	13			8.8
CDB1-847	208.375	23	0	94	
CDB1-845	208.07	49			3.1
CDB1-843	207.23	25	0	97	3.5
CDB1-841	206.645	20	0	97	
CDB1-839	206.005	13			4.9
CDB1-837	205.75	16	2	94	
CDB1-1297	205.405	17	0	98	0.9
CDB1-835	204.88	44			
CDB1-833	204.485	49			0.2
CDB1-831	203.01	41			0.1
CDB1-829	202.15	40	0	87	
CDB1-825	200.73	33	28	64	
CDB1-823	200	31	33	57	
CDB1-821	199.23	29	27	62	0.0
CDB1-819	197.955	32	0	85	0.2
CDB1-817	197.215	36	10	77	
CDB1-1299	196.74	36	21	67	
CDB1-96	196.29	20	12	75	0.2
CDB1-1301	195.775	27	9	79	
CDB1-815	195.405	31	15	76	0.4
CDB1-1303	195.265	35	5	82	
CDB1-1305	195.24	56	5	83	3.2
CDB1-813	195.13	45	10	78	
CDB1-811	194.405	67	0	0	0.7
CDB1-1307	193.84	67			
CDB1-809	193.4	49	10	77	
CDB1-94	193.04	46	0	84	0.5
CDB1-807	192.57	54			
CDB1-1309	192.205	69			
CDB1-1311	191.575	66	10	78	
CDB1-803	190.89	62			0.6
CDB1-1313	190.31	70			
CDB1-801	190.04	60			1.9
CDB1-1315	189.41	54	0	80	
CDB1-799	188.86	74			1.6
CDB1-797	188.33	55	29	60	
CDB1-92	187.54	38	52	41	3.7
CDB1-795	186.895	60	28	61	
CDB1-793	186.45	49	37	51	4.0
CDB1-1317	185.865	49	36	50	

CDB1-91	184.425	45			
CDB1-791		68			11.8
CDB1-789	183.775	78			
CDB1-89	183.475	52	53	32	10.7
CDB1-1319	182.925	45	18	52	
CDB1-783	182.28	71	13	56	3.4
CDB1-781	181.96	42	31	44	
CDB1-1321	181.32	50	5	60	8.2
CDB1-779	180.655	52	58	33	
CDB1-87	180.325	61	64	27	7.2
CDB1-777	179.665	67	69	26	0.7
CDB1-775	179.27	37			
CDB1-1323	178.875	54	69	27	
CDB1-1325	178.37	50	53	38	2.6
CDB1-773	177.835	70	26	62	
CDB1-85	177.415	50	37	49	5.2
CDB1-771	177.045	63	29	58	
CDB1-769	176.53	58	3	78	
CDB1-84	176.105	13	46	44	4.5
CDB1-1327	175.295	39	28	56	
CDB1-765	174.88	56	36	53	1.2
CDB1-763	174.275	24			
CDB1-761	173.775	43			0.2
CDB1-759	172.89	51			
CDB1-755	172.155	31	38	51	
CDB1-753	171.78	37	24	63	
CDB1-751	170.975	41			
CDB1-82	170.28	44			0.4
CDB1-1329	169.485	37			
CDB1-747	168.665	36	25	61	
CDB1-81	167.85	25	9	81	
CDB1-745	167.29	22	43	45	
CDB1-1331	166.75	16			
CDB1-743	165.985	18	29	61	
CDB1-741	165.175	11			
CDB1-1333	164.69	16			
CDB1-739	164.285	13			0.2
CDB1-737	163.59	12			
CDB1-1335	163.075	14	40	49	
CDB1-735	162.3	23	36	53	0.0
CDB1-733	161.835	27	34	55	
CDB1-1337	161.255	32	27	57	
CDB1-731	160.55	37	32	56	0.1
CDB1-1339	159.985	31	24	62	
CDB1-729	159.67	30			
CDB1-1440 E	159.475	20			
CDB1-1440 D	159.46	5	46	40	
CDB1-1440 C	159.415	5			
CDB1-74	159.1	4	42	45	

CDB1-75	159.05	4	48	43	
CDB1-1440 B	159.05	4			
CDB1-1440 A	158.9	4	58	34	
CDB1-727	158.575	41			0.2
CDB1-725	158.16	51	49	41	
CDB1-77	157.925	47			
CDB1-721	156.375	54			0.3
CDB1-72	155.65	17	0	94	
CDB1-1341	155.205	40			
CDB1-719	154.87	52	37	42	1.0
CDB1-717	154.085	53	4	43	
CDB1-715	153.045	68	39	43	
CDB1-1343	152.135	54	62	27	
CDB1-1345	151.36	44	37	53	
CDB1-707	150.425	57	71	25	1.5
CDB1-705	149.175	66	68	30	
CDB1-703	147.86	50	68	25	
CDB1-701	147.675	63	64	31	2.0
CDB1-699	146.57	67	56	39	
CDB1-1347	146.285	62	36	57	
CDB1-695	144.685	56	28	64	
CDB1-693	144.025	69	36	55	3.3
CDB1-68	143.35	78	23	70	
CDB1-691	142.455	28	21	71	
CDB1-689	142.075	74			1.9
CDB1-66	141.23	71			
CDB1-1349	140.7	75			
CDB1-685	139.745	69	1	87	
CDB1-683	138.77	51	5	81	8.2
CDB1-681	137.675	69	8	79	
CDB1-65	136.825	24	16	68	
CDB1-1351	136.085	42	14	74	
CDB1-63	135.4	42			
CDB1-679	134.42	34			
CDB1-677	134.16	35	21	67	
CDB1-675	133.62	32			
CDB1-673	132.98	58			
CDB1-671	132.14	24	2	85	2.1
CDB1-57	131.46	29	11	73	
CDB1-667	130.05	57	23	65	3.6
CDB1-665	129.22	59	0	89	
CDB1-1353	128.035	31			3.9
CDB1-661	127.255	49			
CDB1-659	126.29	63	24	65	2.2
CDB1-55	125.42	30	31	54	
CDB1-655	124.925	56			
CDB1-653	124.22	74			0.2
CDB1-651	123.925	57	33	55	
CDB1-53	122.76	45	27	58	

CDB1-649	122.11	46	7	76	0.0
CDB1-647	121.22	47	38	49	
CDB1-645	120.315	39	26	61	0.2
CDB1-643	119.4	68			
CDB1-641	118.175	33	17	65	1.6
CDB1-1355	117.135	11			
CDB1-637	116.075	34			0.3
CDB1-635	115.125	9			
CDB1-633	114.17	12	45	44	0.2
CDB1-1357	113.605	13			
CDB1-631	113.305	17	20	60	
CDB1-629	112.725	23			0.1
CDB1-47	111.85	13	54	36	
CDB1-627	111.3	17			
CDB1-625	110.93	30	48	41	
CDB1-623	110.17	38			0.1
CDB1-621	109.57	23	30	48	
CDB1-619	108.82	25	7	71	
CDB1-617	108.05	18			0.1
CDB1-46	107.4	23	29	52	
CDB1-1359	106.85	32			3.9
CDB1-1361	106.79	25	42	43	
CDB1-615	106.695	25	24	43	
CDB1-44	106.475	20	18	45	
CDB1-613	105.29	63	25	57	1.2
CDB1-611	104.665	50			
CDB1-609	103.335	67			0.5
CDB1-605	101.88	51			4.7
CDB1-603	100.725	57	56	33	
CDB1-601	100.13	65	47	36	
CDB1-599	99.29	63	18	71	0.3
CDB1-597	98.24	58	63	22	
CDB1-595	96.755	55	45	40	1.1
CDB1-593	95.7				1.8
CDB1-1363	95.34	70	52	35	
CDB1-591	94.715	42			
CDB1-589	93.875	51	41	45	5.0
CDB1-1365	92.585	57			
CDB1-1367	91.375	17	50	34	5.0
CDB1-579	90.57	14	42	46	
CDB1-1369	90.335	44	63	29	
CDB1-577	89.56	51			
CDB1-1371	89.48	48	50	35	
CDB1-575	88.82	43			3.1
CDB1-573	87.625	49	48	40	6.1
CDB1-39	86.775	38	32	57	
CDB1-571	85.895	61	64	26	0.4
CDB1-1373	85.685	52	5	56	
CDB1-569	84.3	56	43	29	

CDB1-1438	85.13	14	78	16
CDB1-566	85.1	16	56	31
CDB1-583	84.09	52		
CDB1-565	83.425	78		
CDB1-37	83.275	29		
CDB1-563	83.2	57		
CDB1-1375	82.855	63		
CDB1-559	82.58	53		
CDB1-1377	82.28	58		
CDB1-557	82.07	43		
CDB1-1379	81.82	57		
CDB1-1381	81.605	54		
CDB1-1383	81.455	52		
CDB1-1385	81.165	59		
CDB1-1387	80.945	48		
CDB1-555	80.725	49		
CDB1-1389	80.455	54		
CDB1-553a	80.25	64		
CDB1-553	80.18	46		
CDB1-1391	79.775	54		
CDB1-549	79.56	49		
CDB1-1393	79.375	44		
CDB1-1395	79.155	48		
CDB1-1397	78.935	48		
CDB1-1399	78.72	62		
CDB1-547	78.625	47		
CDB1-29	78.525	26		
CDB1-545	78.105	56		
CDB1-1401	77.935	39		
CDB1-543	77.71	49		
CDB1-1403	77.445	45		
CDB1-1405	77.23	42		
CDB1-1407	76.445	44		
CDB1-1409	76.265	52		
CDB1-27	76.025	7		
CDB1-1411	75.855	55		
CDB1-541	75.825	33		
CDB1-1413	75.61	41		
CDB1-539	75.32	40		
CDB1-1415	75.135	44		
CDB1-1417	74.925	39		
CDB1-537	74.64	31		
CDB1-1419	74.405	32		
CDB1-1421	74.16	69		
CDB1-1423	74.03	40		
CDB1-535	73.84	15		
CDB1-1425	73.615	34		
CDB1-1427	73.345	38		
CDB1-533	73.21	42		

CDB1-26	72.85	50
CDB1-1429	72.585	41
CDB1-531	72.4	22
CDB1-529	72	17
CDB1-1431	71.62	9
CDB1-1433	71.225	38
CDB1-1435	71.075	75
CDB1-25	70.9	60
CDB1-525	70.07	30
CDB1-1437	69.305	38
CDB1-23	68.375	13
CDB1-521	67.75	42